ADVANCED MATERIALS
www.advmat.de

Proximity-Mediated Multi-Ferroelectric Coupling in Highly Strained EuO-Graphene Heterostructures

Satakshi Pandey, Thomas Pin, Simon Hettler, Raul Arenal, Corinne Bouillet, Thomas Maroutian, Jérôme Robert, Benoit Gobaut, Bohdan Kundys, Jean-François Dayen, and David Halley**

2D van der Waals materials and their heterostructures are a fantastic playground to explore emergent phenomena arising from electronic quantum hybridization effects. In the last decade, the spin-dependant hybridization effect pushed this frontier further introducing the magnetic proximity effect as a promising tool for spintronic applications. Here the uncharted proximity-controlled magnetoelectric effect in EuO/graphene heterostructure is unveiled. This is obtained while creating a new multiferroic hybrid heterostructure with multifunctional properties. Using a topotactic method magnetic insulating EuO thin films on graphene is grown under high compressive strain, which induces the appearance of an additional ferroelectric order, with an electric polarization that reaches up to 18 μC cm^{-2} at room temperature. This observation therefore quantitatively confirms the theoretical predictions made 15 years ago of a strain-induced ferroelectric state in EuO. Moreover, the EuO induces a magnetic proximity state into the graphene layer by interfacial hybridization. This new ferroelectric state in the EuO/graphene heterostructure is stable up to room temperature where it coexists with the EuO/graphene magnetic state. Furthermore, intertwined magneto-electric effects are shown in these strained heterostructures which can facilitate the manipulation of magnetization and electric polarization in future memory and neuromorphic devices.

1. Introduction

Coupling different functionalities in the same material phase has attracted a lot of attention in the last decade, paving the way to pioneer physical phenomena and novel device applications. In particular, the combination of magnetic and electric orders in multiferroic materials is of the highest interest. These multiferroic materials,[1] when exhibiting magneto-electric properties,[2] are being used for the next generation of spintronic and memory devices, with additional possibilities opened by the mutual control of electric[3] and magnetic[4] properties.

On the fundamental side, magnetoelectric materials are fascinating systems driven by symmetry-breaking mechanisms, Berry phase physics, and spin-orbit coupling.[5–7] When going at the 2D scale, and because of their ultimate interfacial coupling conditions, novel multiferroic coupling effects are expected.[8] Moreover, novel properties are expected in the flatland while taking advantage of the hybridization of graphene with ferroic materials.[9,10] In particular, theoretical calculations by Ibrahim et al.[11] unveiled that an intriguing multiferroic proximity effect can be imprinted into a graphene layer when it is properly interfaced with a multiferroic material. The authors exploited this novel phenomenon further and proposed a new concept of spin-valve. In such a so-called proximity multiferroic resistance device, multiple memory states could be encoded into the graphene

S. Pandey, T. Pin, J. Robert, B. Gobaut, B. Kundys, J.-F. Dayen, D. Halley
Institut de Physique et Chimie des Matériaux de Strasbourg
Université de Strasbourg, CNRS
UMR 7504, Strasbourg F-67000, France
E-mail: jean-francois.dayen@ipcms.unistra.fr, dayen@unistra.fr; david.halley@unistra.fr

The ORCID identification number(s) for the author(s) of this article can be found under https://doi.org/10.1002/adma.202417669

DOI: 10.1002/adma.202417669

S. Hettler, R. Arenal
Laboratorio de Microscopias Avanzadas (LMA)
Universidad de Zaragoza
Zaragoza 50018, Spain

S. Hettler, R. Arenal
Instituto de Nanociencia y Materiales de Aragon (INMA)
CSIC-Universidad de Zaragoza
Zaragoza 50018, Spain

R. Arenal
Araid Foundation
Zaragoza 50018, Spain

C. Bouillet
Plateforme MACLE-CVL UAR2590
1b, rue de la Férollerie, Orléans Cedex 2 45071, France

T. Maroutian
Centre for Nanoscience and Nanotechnology, CNRS
Universite Paris-Saclay
Palaiseau F-91120, France

resistance upon switching independently the electric polarization and/or the magnetization states of the multiferroic material.

On the applied side, the increasing energy consumption of information and communication technologies such as in neuromorphic and logic applications,[12,13] requires new paradigms for calculating and storing information, in a non-volatile way, with much more energy-efficient operation. In this context, the coupling of ferroelectricity with spintronic concepts is promising as it combines the advantages of high endurance, low energy consumption, and fast operability.[14] Moreover, it opens the doors to new device concepts while playing with the two degrees of freedom in memory or logic devices through bias voltage and magnetic field.

The number of multiferroic materials, available at room temperature, is nevertheless limited. In order to enlarge the panel of these materials, strain appears as an efficient tool: the high reachable strain in thin layers or nanowires can modulate the properties of some materials relative to their bulk state and force them into a multiferroic phase. This strain effect has been extensively studied in perovskite, in order to bring for instance $BiFeO_3$,[15,16] or $EuTiO_3$[17,18] into an exploitable ferroelectric (FE) state. Less attention has been paid to strain in binary oxides – among which the doping effect in ferroelectric HfO_2[19] attracted more interest – but some theoretical papers suggested that a high strain should favor the appearance of a ferroelectric state in ferromagnetic rock-salt structures as BaO[20,21] or EuO[22,23] which are paraelectric in the unstrained state.[23,24] Bousquet et al.[22] demonstrated, from DFT calculations, that, above a given biaxial strain threshold (−3% in compression, 4% in tension), EuO should exhibit a large tetragonalization and a non-negligible electric polarization which strongly increases with the strain value. This effect was indirectly experimentally observed in epitaxial EuO layers in EuO/BaO stacks under tensive strain[25] through optical techniques, but the electric polarization in EuO has not been assessed as far as we know – to the best of our knowledge.

In the present article, we show that the large compressive strain reached in our EuO/ graphene heterostructures, grown by an original method, drives EuO into a ferroelectric state, with a large polarization close to 18 μC cm^{-2} at room temperature. This observed ferroelectric state coexists at room temperature with the magnetic state recently demonstrated in such systems.[26] The coexistence of these two order parameters, combined with the lateral transport properties of the graphene layer[27,28] that are potentially influenced by the proximity of EuO,[26] makes such a system appealing for applications, all the more as we also demonstrate here magneto-electric effects, with a clear influence of the magnetic field on the electric polarization. The present article focuses on the properties of EuO layers, influenced by the underlying graphene layer, but we have to keep in mind the potential role that graphene itself could play as a spin transport medium.[29,30]

2. Strained EuO State

As detailed in the method part, we grow smooth continuous layers (**Figure 1c**) of polycrystalline EuO on graphene[26] through a topotactic technique based on the reduction of the Eu_2O_3 thin film by a top Ti capping.[31] Provided that the initial Eu_2O_3 layer is not thicker than 8 nm, the whole initial layer turns into the EuO phase. Above this threshold thickness, an 8 nm EuO layer is obtained on top of a residual and amorphous not reduced Eu_2O_3 layer (Figure 1e).[26] For more details and TEM observations, the reader can go to ref. [26] where the amorphous/crystalline structure of Eu_2O_3/Eu is systematically characterized The topotactic technique turns out to be an excellent way of preparing EuO films since it does not require delicate epitaxial growth techniques[32,33] that could preclude industrial applications. As expected the EuO film demonstrates clear ferromagnetic properties with an in-plane easy axis, as revealed by SQUID measurements (Figure 1a). In addition, a magnetic state is induced into the graphene by the proximity effect[34] as indicated by anomalous Hall effect measurements (Figure 1b), and predicted theoretically.[35,36] For additional specific information on the magnetic properties of topotactic EuO/Gr heterostructure, the reader can refer to our previous dedicated work.[26]

X-ray diffraction measurements provide information on the film structure (Figure 1d): Besides a strong Eu_3O_4 (220) peak associated with clusters positioned in the EuO matrix, below the Ti layer (which is intense, because all, well oriented, Eu_3O_4 grains contribute to the Bragg peak), we observe a polycrystalline EuO layer (with intense (111) and (200) peaks), and no Eu_2O_3 peaks (as expected for samples thinner than 8 nm). A series of samples with an increasing thickness of deposited Eu_2O_3 (Figure 1d,f) shows that EuO on graphene is in a compressive state, that partially relaxes as the thickness is increased: surprisingly, the out-of-plane lattice parameter does not tend to the bulk value (a_{bulk} = 5.145 Å) as the thickness increases, but seems to saturate at a misfit of 2.7% and 2.1% for (111) and (200) peaks. The shape of the curves indeed suggests that the relaxation almost ends above 10 nm; this may be related to the fact that Eu_2O_3 is not reduced into EuO if the thickness exceeds 8 nm: above this value, an amorphous layer of Eu_2O_3 remains between graphene and EuO which might freeze the strain relaxation process.

The remaining out-of-plane strain at a thickness of 8 nm (thickness of the characteristic samples that we will study below) reaches 4.4% and 3.4% for respectively (111) and (200) peaks (Figure 1f). In order to assess the in-plane biaxial strain, we need a precise knowledge of the EuO Poisson coefficient ν, that was, to our knowledge, only theoretically evaluated: Bousquet et al.[22] predicted, in the case of EuO/BaO system, ν in the order of 0.58 in the paraelectric state and 0.33 in the ferroelectric state. In the paraelectric hypothesis, we would therefore reach between −2.6% and −2.0% for the compressive biaxial strain. Taking into consideration the threshold strain values calculated by Bousquet et al. for the appearance of ferroelectricity (4% in expansion, −3% in compression) we conclude that the experimental values of strain are close to them, and even higher for the out-of-plane strain: We therefore reach the strain regime for which a ferroelectric state should appear.

We have moreover to underline the role played by graphene in the appearance of this high strain: When deposited onto SiO_2, without graphene (Figure 1f), EuO films exhibit a lower strain level, especially for thin layers with the out-of-plane strain of 3.6% instead of 5.5% for (111) and of 2.4% instead of 3.9% for (200)). As will be shown below, this difference in strain is crucial for the appearance of the ferroelectric state at high temperature, which makes graphene an appropriate template also for mechanical reasons. The different stresses in EuO layers grown on SiO_2 or on graphene may have different origins: A difference

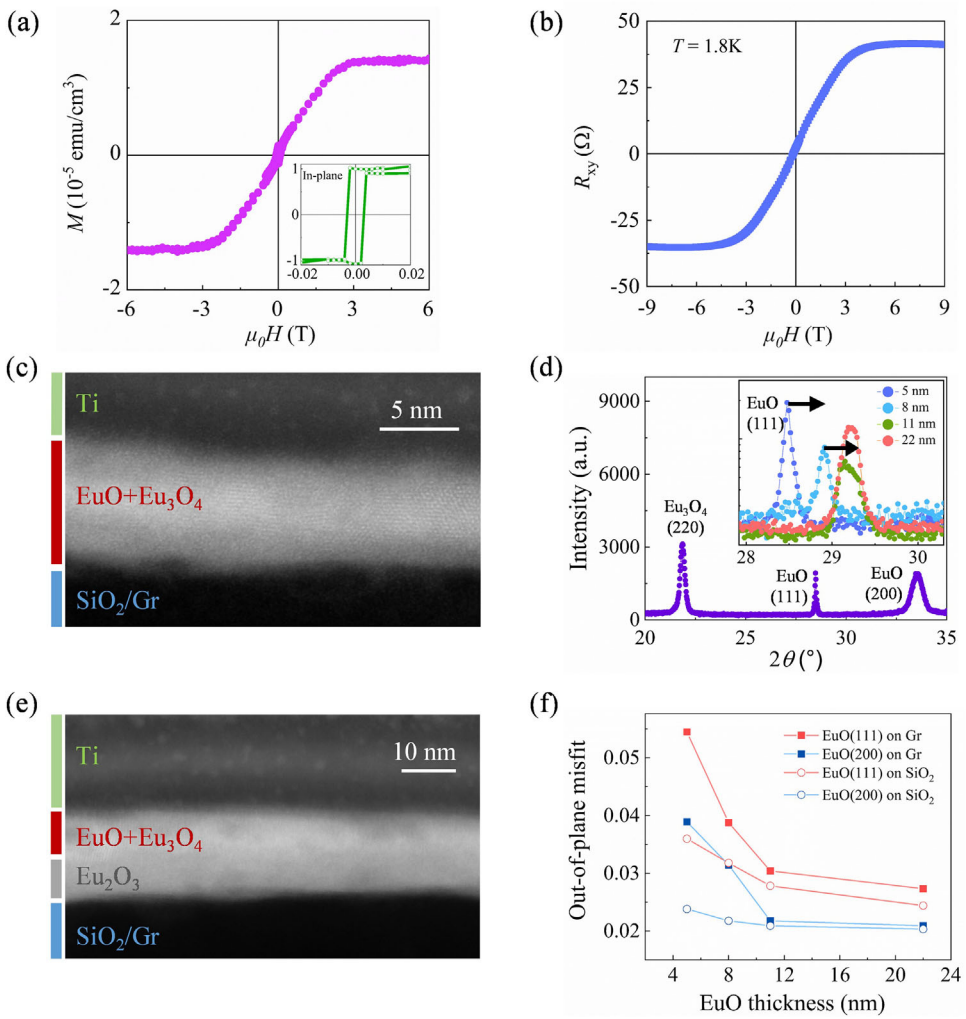

Figure 1. EuO film under compressive strain grown on graphene by a topotactic method. a) SQUID *M(H)* out-off plane measurement at 10 K. Inset: SQUID *M(H)* in plane measurement at 35 K. b) as-measured $R_{xy}(H)$ transverse resistance at 1.8 K. c) Scanning transmission electron microscopy image of a cross-section showing the SiO_2 substrate and the Ti capping layer surrounding a 7 nm thick europium oxide layer with, nanocrystalline EuO with Eu_3O_4 clusters in the top part. d) X-ray diffraction of a 5 nm thick sample grown on graphene. Inset: EuO (111) Bragg peak measured for different layer thicknesses, showing a large strain relaxation with increasing thickness. The thickness of the EuO layer does not show an influence on the width of Bragg peaks (which should however not modify the estimation of the strain from the Bragg angle). e) Cross section of a 15 nm thick layer showing crystalline EuO including Eu_3O_4 clusters in the top part, and below, amorphous Eu_2O_3. f) Lattice strain relative to bulk EuO, obtained from (200) and (111) Bragg peaks as a function of thickness for samples grown on graphene (Gr) or directly on SiO_2. The asymptotic strain values on graphene are indicated (dotted lines).

in the microstructure (roughness, defects, etc.) in Eu_2O_3 grown on graphene could induce a difference during the crystallization of EuO from the top interface. Alternatively, the different thermal expansion coefficients in graphene and SiO_2 (respectively -8×10^{-6} K^{-1} and 5.5×10^{-5} K^{-1}) [37,38] may lead to differences in the residual strain after the annealing step.

We now move on to investigate the electrical signatures of the strained EuO/Gr heterostructure while performing careful temperature-dependent vertical transport measurements.

3. Ferroelectric EuO State

The temperature-dependent study of the capacitance signal reveals the apparition of a clear transition mechanism to another polar state below $T_1 = 37$ K. This transition is also confirmed by a classical peak in the dielectric loss testifying for dipoles rearrangement into a more thermodynamically favorable configuration (**Figure 2**b (inset)). In order to investigate further the mechanism at play and identify the electric phases of the material, the DC-voltage-dependent behavior *C(V)* is investigated on each side of the transition, revealing striking distinct electrical phases:

- Below T_1 (Figure 2c), the *C(V)* trace is characteristic of a transition from an anti-ferroelectric (AFE) state[39] at low voltage to a ferroelectric state at higher voltage for both voltage polarities: the capacitance increases smoothly with increasing *V* and does not exhibit a hysteresis at low voltage; above (below) a given threshold close to +15 V resp. −15 V), *C* increases rapidly with

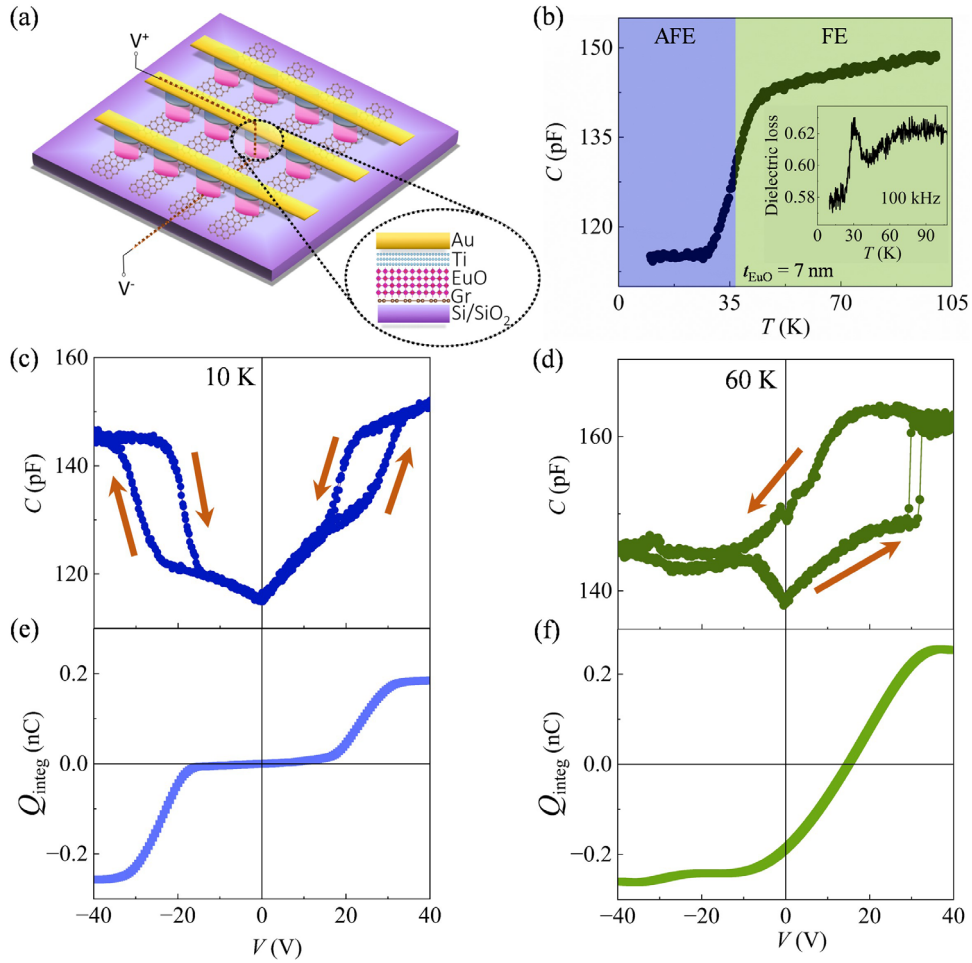

Figure 2. Ferroelectric transition on strained EuO/graphene heterostructures: Capacitive measurements at low temperature on a 7 nm thick EuO film grown on graphene. The measurement frequency is 3.10^5 Hz. a) Scheme of the devices. b) *C(T)* curve and dielectric loss (inset) measured at $V = 0$ with a 50 mV AC voltage, showing a transition around $T_1 = 37$ K (taken at the inflection point). c) *C(V)* curve at 10 K with a transition from an AFE to a FE state. d) *C(V)* curve at 60 K showing an FE state. e,f) Electric charge corresponding to the integrated hysteresis of the capacitance as a function of voltage in (c) and (d).

V and an anticlockwise (resp. clockwise) hysteretic loop opens on the positive (resp. negative) side. The polarized hystereses are clear signatures that the oxide turned into a ferroelectric state; Consistently, for higher voltages exceeding the coercive voltage, *C* remains constant, and the loop closes as the polarization saturates

- Above T_1 (Figure 2d) a unique anticlockwise *C(V)* hysteresis loop is observed. It expands around $V = 0$ V on each polarity side and closes around $V = \pm 30$ V beyond which *C* saturates. This proves a ferroelectric behavior with slightly asymmetric coercive electric fields.

Regarding now the high-temperature range, we measured the *C(T)* curve shown in **Figure** 3a, performed on a similar 7 nm thick sample, up to 300 K (and even up to 380 K see Figure S1, Supporting Information). This *C(T)* curve confirms the AFE-FE transition near $T_1 = 37$ K, above which the capacitance of EuO in the ferroelectric state slowly increases and then follows a plateau with a very slight maximum near 220 K. In the high-temperature range, the shape of the hysteretic *C(V)* curves shows a dip close to low voltage range indicating the cross of the charge neutrality point (The reader can also see Figure S4b (Supporting Information) in which the Dirac point in graphene below EuO is evidenced through transconductance measurements, showing a decrease of the lateral current – and thus of the electric charge at the graphene/EuO interface around the neutrality point). Then, above a threshold in the order of $V = -10$ V and $V = +10$ V, the hysteresis closes and *C* follows a saturated linear behavior with *V*. The plot of the hysteresis value, integrated as a function of voltage, (Figure 3e and also Figure S2c, Supporting Information) follows the usual voltage-dependent behavior of a ferroelectric polarization switch, between clear saturation states. Moreover, *G(V)* curves (the leakage through the EuO layer) exhibit a similar hysteretic behavior (Figure 3d,f; Figure S2a, Supporting Information) closely related to the hysteresis observed on *C(V)* plots: this analogy pleads for an electro-resistive effect[40,41] and is again related to the switch of the ferroelectric polarization in the polycrystalline EuO layer.

Furthermore, piezoresponse force microscopy (PFM) (Figure 3b) shows the response of a similar 7 nm thick EuO

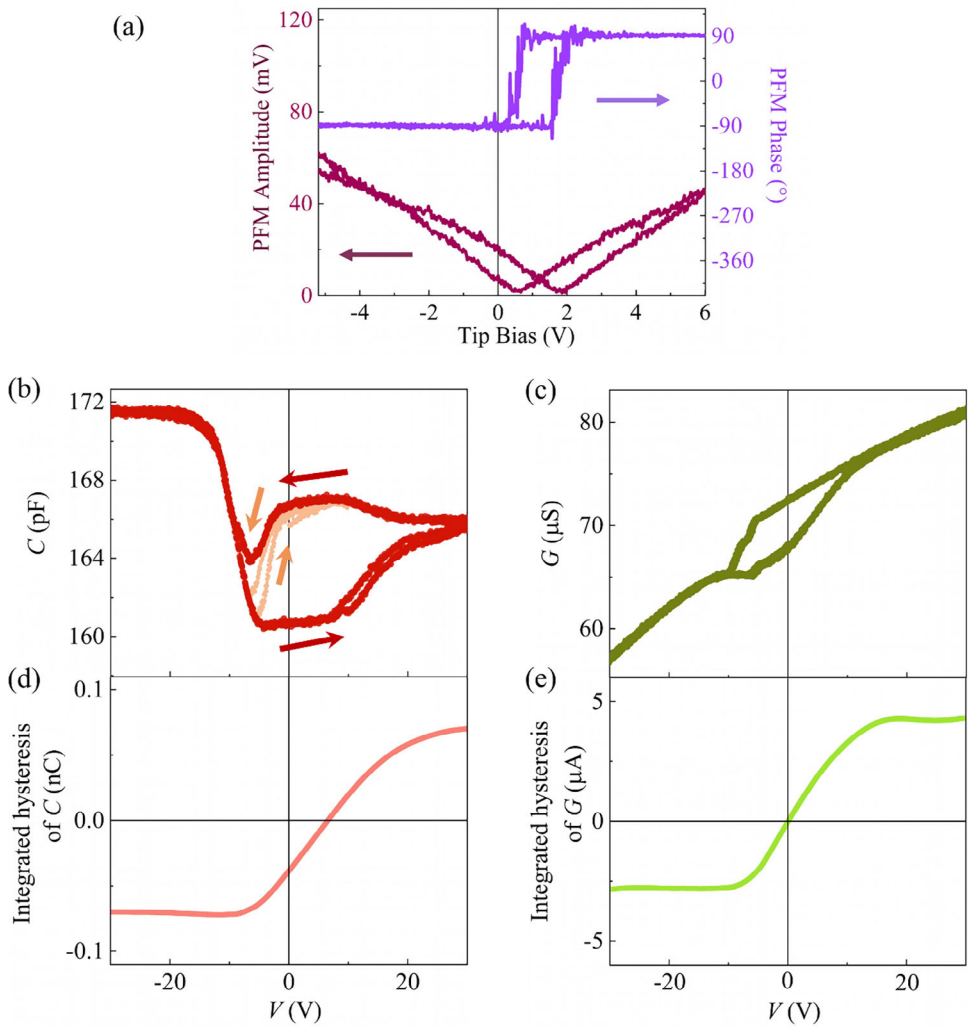

Figure 3. a) PFM observation (amplitude and phase) showing a full reversal of the out-of-plane deformation of EuO as a function of the applied bias voltage (which precludes writing of domains of opposite signs). b) *C(V)* curve showing an FE state. Orange curve: minor loop from −10 V to +10 V. c) *G(V)* curve measured through the EuO layer. d) Charge corresponding to the integrated hysteresis of the red curve in (b). e) Current corresponding to the integrated hysteresis of the curve in (c).

sample that reveals a hysteresis behavior typical for polarization switching and is consistent with our *C(V)* observations of a ferroelectric state. In the phase loop, we observe a relative shift of 180° indicating the full reversal of the out-of-plane response with the applied voltage. This is in support of a polarization aligned parallel to the applied electric field. The whole hysteresis loop is shifted toward positive voltage values by ≈1 V, which indicates a built-in electric field oriented upward inside the EuO film.

Quantitative estimations of the ferroelectric polarization at room temperature are obtained from the capacitance measurements: For 7 nm thick EuO samples and 20 μm diameter junctions, from the integration of the hysteretic part of *C* relative to the voltage *V* (Figure 3e; Figure S2c, Supporting Information) we assess a minimum value of *P* (considering only the hysteretic contribution) which is ≈18 μC cm^{-2}. This value shows a remarkable match with the predictions of Bousquet et al.[22]: Thus, according to these calculations, a ferroelectric polarization of 18 μC cm^{-2} would be reached for a compressive strain of -4%, and an extensive strain slightly above 5%. This last value is in consistent agreement with the out-of-plain strain measured on our film (see X-ray diffraction measurements in Figure 1d).

Observations made on thicker EuO layers (Figure S3, Supporting Information), with a more relaxed biaxial strain, show that the electric polarization is reduced in such samples and that the Curie ferroelectric transition is pushed down to ≈180 K: this again confirms the predictions of Bousquet et al. of a strain-induced ferroelectric state in our thin EuO layers, with a clear correlation between thickness, strain and ferroelectric polarization.

We moreover show in Figure S4 (Supporting Information) that the observed ferroelectric polarization in EuO can noticeably influence the lateral electronic transport in graphene (at least at low temperature), with typical transconductance loops (Figure S4b, Supporting Information) that are supplementary proofs of the strain-induced ferroelectric state in EuO.

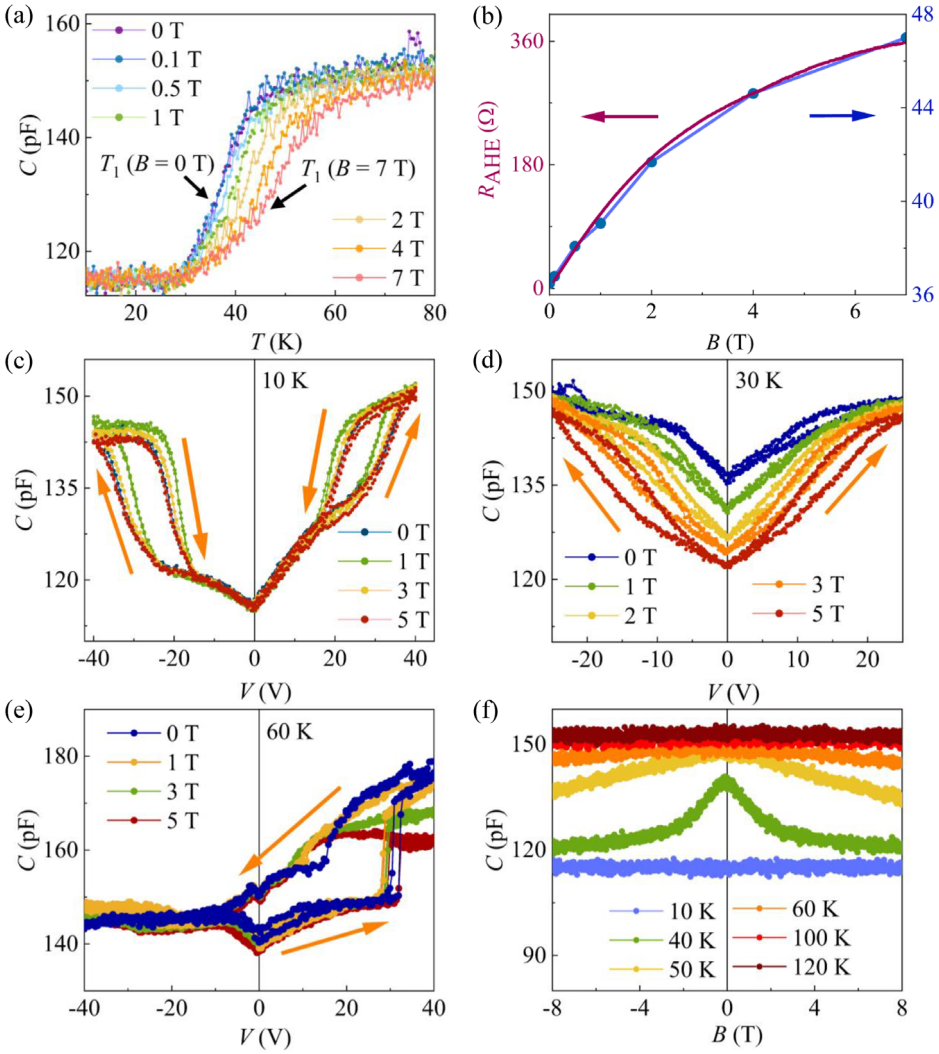

Figure 4. a) *C(T)* curves measured around $V = 0$ V on a 7 nm thick sample under different out-of-plane magnetic fields *B*. b) Transition temperature T_1 (blue curve, right) as a function of *B*, and Anomalous Hall Effect Resistance (red curve, left) measured at 40 K showing the slowly saturating magnetization behavior. The scales are chosen to highlight the similar dependency on *B* of both quantities. c–e) Influence of *B* on *C(V)* curves: (c) and (d) *C(V)* curves measured below T_1 and (e) above T_1, for different magnetic fields. The asymmetry of the loops shifted to positive voltages and centered ≈+15 V, is consistent with PFM observations and reflects the asymmetry of the electrodes (graphene at the bottom and Ti at the top) on both sides of EuO. f) *C(B)* curves at different temperatures, with a large amplitude bell-shaped peak for $T = T_1$.

4. Magneto-Electric Effect in EuO

We demonstrated above the presence of ferroelectric polarization in EuO up to room temperature. It is remarkable as such a system is also magnetic above room temperature. For more details concerning the magnetic characterization of our EuO layers (from 2K to 380 K), the reader can see in [Pandey. et al. [26]]). We have to investigate the possibility of magneto-electric effects that are mostly expected in such multiferroic systems.[1,42] If magneto-electric effects are present, this coupling between *M* and *P*, should make that an applied magnetic field *B* would not only influence the direction of *M*, but, as a consequence, the direction of *P*. A magnetoelectric effect was analytically predicted by Eliseev et al.[20,43] in EuO-like oxides, when submitted to huge stress that could be reached in nanotubes or nanospheres, but no experimental confirmation of a magneto-electric effect in EuO was nevertheless reported in the literature up to now if we do not consider the extrinsic effect that was shown by Cao et al. in hybrid $BaTiO_3$/EuO structures.[44]

This influence of a magnetic field on the electric polarization behavior is clearly observed in **Figure 4**: When applying an out-of-plane magnetic field, the AFE-FE transition temperature T_1 is pushed to higher values. The plot of $T_1(B)$ (Figure 4b) illustrates this effect: the dependency is not linear, but reminds the shape of *M(B)* curves obtained on such samples.[26] We observe that $T_1(B)$ follows exactly the anomalous Hall effect at 40 K (i.e., close to T_1), which is proportional to the out-of-plane magnetization value. This pinpoints that *P* interacts with *M* and not directly with *B*: at high *B* values the out-of-plane magnetization tends to saturate, and the influence of *B* on *P* as well.

Another illustration of the magneto-electric effect is shown in Figure 4c–e: The shape of the *C(V)* curves is only slightly modified under a magnetic field, far away from the T_1 transition temperature but strongly modified around T_1, with a systematic increase of the hysteresis (Figure 4d). This magneto-electric effect is confirmed (Figure 4f) by *C(B)* curves: at low temperatures, the effect of *B* is negligible, whereas the effect becomes large in the vicinity of the transition temperature T_1 with a nearly symmetric bell-shape decrease of *C* with *B*. Above T_1, the effect of a magnetic field is much weaker, but we still observe a decrease of *C* with *B* up to at least 120 K.

These observations show that, due to the magneto-electric (M.E.) coupling, applying a magnetic field partially aligns some magnetic dipoles and therefore freezes some of the coupled electric dipoles in EuO, which can then no longer contribute to the layer capacitance. This M.E. effect is enhanced close to T_1 where fluctuations in the AFE state might allow small areas of FE domains to appear, that are more sensitive to the magneto-electric influence due to their low size.

The sign of the magneto-electric coupling is a priori not known; *P* could for instance be favored along *M* or perpendicular to it. Nevertheless, we have to notice that the application of a magnetic field out of plane contributes to stabilizing the electric polarization out-of-plane: indeed, the voltage-dependent hysteresis increases upon applying *B* (Figure 4d), proving an increased barrier energy for the polarization reversal. Consequently, we can conclude that the M.E effect might tend to favor the parallel orientation of *P* and *M*.

5. Conclusion

We showed that the biaxial strain in EuO thin layers grown on graphene is high enough to reach the elusive strain threshold calculated by Bousquet et al.,[22] above which EuO turns into a tetragonal, ferroelectric phase: the ferroelectric polarization in 7 nm thick films is preserved up to room temperature as demonstrated by transport and PFM analysis, where it reaches at least 18 μC cm^{-2}. Detailed transport analysis revealed additional intriguing anti-ferroelectric to ferroelectric phase transition at low temperatures. Moreover, magnetoelectric coupling effects were investigated and revealed to be amplified close to the AFE-FE transition temperature.

In such thin films, the coexistence at room temperature of the strong ferroelectric polarization and of a large magnetization, as well as the magnetic and electric proximity effects induced in graphene by those EuO states makes this system extremely interesting for device applications combining charge and spin such as Magneto-Electric Spin–Orbit logics. These results motivate exploring further the potential of van der Waals hybrids for the engineering of complex multifunctional materials taking advantage of quantum hybridization effects for spintronics and ferroelectric applications.

6. Experimental Section

Growth and Magnetic Properties: The sample growths were performed on commercially available substrates (Graphenea) made of a monolayer chemical vapor deposition (CVD) graphene transferred on SiO_2/Si substrate. The samples were out-gassed in an ultra-high vacuum for two hours at 400 °C in a 10^{-10} mBar base pressure in order to get rid of surface contamination such as polymer residues from the CVD transfer process.[45] The deposition of Eu_2O_3 was made at room temperature using an *e*-beam evaporation gun in a molecular beam epitaxy (MBE) chamber, controlled by a quartz microbalance. After deposition, the samples were heated to 450 °C and capped in situ by a 2.5 nm thick titanium layer (Figure 1a,b).[31] The samples were left 40′ at 450 °C after Ti deposition in order to promote the reduction process by titanium of Eu_2O_3 into EuO.

It was shown recently, using this original growth technique that in such heterostructures the EuO magnetic behavior relative to bulk, unstrained EuO, which is ferromagnetic up to T_C = 69 K and paramagnetic above[46–48] was modified: Indeed, it was shown[26] that a superparamagnetic state, due to magnetic polarons[49–51] in strained EuO on graphene, survives above T_C up to 350 K and induced anomalous Hall effect in graphene due to spin proximity effects.[52]

Process of Devices: Vertical junction cross-bar arrays were fabricated for capacitance measurements with a typical junction diameter of tens of micrometers made of the graphene/EuO/Au vertical stack. The bottom graphene electrodes were fabricated by combining standard laser lithography techniques and graphene etching by oxygen plasma.[53,54] After this step, EuO films are grown on top of the patterned graphene stripes using an *e*-beam gun via the topotactic technique as described previously. The top gold electrodes were designed by laser lithography followed by a lift-off process (Figure 2a).

Measurements on capacitance devices made of a 7 nm thick EuO layer show relatively high resistance in the order of 10 to 40 kΩ (see Figure S3a, Supporting Information for conductance values). This enables us to perform precise AC measurements of the capacitance signature of the EuO spacer (Figure 2a). A background capacitance value in the order of 100 pF adds to the capacitive signal and is superposed in devices without EuO layers.

Piezoresponse Force Microscopy (PFM): PFM measurements were performed at room temperature with a Bruker Icon system, using Pt/Cr-coated silicon tips (Multi75E, BudgetSensors) operated ≈15 kHz below the contact resonance frequency (≈330 kHz). The applied AC voltage was 1.5 V for all measurements.

Supporting Information

Supporting Information is available from the Wiley Online Library or from the author.

Acknowledgements

The authors thank the STnano clean room facility and the XRD platform of IPCMS for technical support as well as the Labex NIE for partial support. R.A. and S.H. acknowledge funding from the European Union's Horizon 2020 research and innovation program under the Marie Sklodowska-Curie grant agreement number 889546, the Government of Aragon (DGA) through the project E13 23R, the Spanish MICIU with funding from European Union Next Generation EU (PRTR-C17.I1) promoted by the Government of Aragon and by the Spanish MICIU (PID2019-104739GB-100/AEI/10.13039/501100011033, PID2023-151080NB-I00/AEI/10.13039/501100011033 and CEX2023-001286-S MICIU/AEI /10.13039/501100011033). This study was supported by French state funds managed by the ANR more specifically within the grants MixDferro (ANR-21-CE09-0029) and 2DSwitch (ANR-21-CE09-0031). J.-F.D. also acknowledges a Junior grant from Institut Universitaire de France.

Conflict of Interest

The authors declare no conflict of interest.

Data Availability Statement

The data that support the findings of this study are available from the corresponding author upon reasonable request.

Keywords

electric polarization, europium oxide, graphene, magneto-electric effect, multiferroicity

Received: November 14, 2024
Revised: February 21, 2025
Published online: March 13, 2025

[1] N. A. Spaldin, M. Fiebig, *Science* **2005**, 391, https://doi.org/10.1126/science.1113357.
[2] R. Ramesh, N. A. Spaldin, *Nature Mater* **2007**, *6*, 21.
[3] T. Kimura, T. Goto, H. Shintani, K. Ishizaka, T. Arima, Y. Tokura, *Nature* **2003**, *426*, 55.
[4] R.-Q. Wang, Y.-W. Fang, T.-M. Lei, *J. Magn. Magn. Mater.* **2023**, *565*, 170297.
[5] D. Vanderbilt, *Berry Phases in Electronic Structure Theory: Electric Polarization, Orbital Magnetization and Topological Insulators*, Cambridge University Press, Cambridge, **2018**.
[6] M. Dawber, K. M. Rabe, J. F. Scott, *Rev. Mod. Phys.* **2005**, *77*, 1083.
[7] M. Fang, W. Zhang, X. Wu, W. Guo, H. Xia, Y. Wang, W. Wang, J. Shen, *APL Mater.* **2021**, *9*, 060704.
[8] T. Zhong, X. Li, M. Wu, J.-M. Liu, *Natl. Sci. Rev.* **2020**, *7*, 373.
[9] V. Zatko, R. Galceran, M. Galbiati, J. Peiro, F. Godel, L.-M. Kern, D. Perconte, F. Ibrahim, A. Hallal, M. Chshiev, B. Martinez, C. Frontera, L. Balcells, P. R. Kidambi, J. Robertson, S. Hofmann, S. Collin, F. Petroff, M.-B. Martin, B. Dlubak, P. Seneor, *Nano Lett.* **2023**, *23*, 34.
[10] B. Yang, B. Bhujel, D. G. Chica, E. J. Telford, X. Roy, F. Ibrahim, M. Chshiev, M. Cosset-Chéneau, B. J. van Wees, *Nat. Commun.* **2024**, *15*, 4459.
[11] F. Ibrahim, A. Hallal, D. S. Lerma, X. Waintal, E. Y. Tsymbal, M. Chshiev, *2D Mater.* **2019**, *7*, 015020.
[12] R. Ramesh, S. Salahuddin, S. Datta, C. H. Diaz, D. E. Nikonov, I. A. Young, D. Ham, M.-F. Chang, W.-S. Khwa, A. S. Lele, C. Binek, Y.-L. Huang, Y.-C. Sun, Y.-H. Chu, B. Prasad, M. Hoffmann, J.-M. Hu, Z. (Jackie) Yao, L. Bellaiche, P. Wu, J. Cai, J. Appenzeller, S. Datta, K. Y. Camsari, J. Kwon, J. A. C. Incorvia, I. Asselberghs, F. Ciubotaru, S. Couet, C. Adelmann, et al., *APL Mater.* **2024**, *12*, 099201.
[13] A. Mehonic, C. Frenkel, E. Vasilaki, *Neuromorph. Comput. Eng.* **2023**, *3*, 040201.
[14] J. Puebla, J. Kim, K. Kondou, Y. Otani, *Commun. Mater.* **2020**, *1*, 24.
[15] Y.-L. Huang, D. Nikonov, C. Addiego, R. V. Chopdekar, B. Prasad, L. Zhang, J. Chatterjee, H.-J. Liu, A. Farhan, Y.-H. Chu, M. Yang, M. Ramesh, Z. Q. Qiu, B. D. Huey, C.-C. Lin, T. Gosavi, J. Íñiguez, J. Bokor, X. Pan, I. Young, L. W. Martin, R. Ramesh, *Nat. Commun.* **2020**, *11*, 2836.
[16] P. Meisenheimer, G. Moore, S. Zhou, H. Zhang, X. Huang, S. Husain, X. Chen, L. W. Martin, K. A. Persson, S. Griffin, L. Caretta, P. Stevenson, R. Ramesh, *Nat. Commun.* **2024**, *15*, 2903.
[17] J. H. Lee, L. Fang, E. Vlahos, X. Ke, Y. W. Jung, L. F. Kourkoutis, J.-W. Kim, P. J. Ryan, T. Heeg, M. Roeckerath, V. Goian, M. Bernhagen, R. Uecker, P. C. Hammel, K. M. Rabe, S. Kamba, J. Schubert, J. W. Freeland, D. A. Muller, C. J. Fennie, P. Schiffer, V. Gopalan, E. Johnston-Halperin, D. G. Schlom, *Nature* **2010**, *466*, 954.
[18] A. Bussmann-Holder, E. Liarokapis, K. Roleder, *Sci. Rep.* **2021**, *11*, 18978.
[19] U. Schroeder, M. H. Park, T. Mikolajick, C. S. Hwang, *Nat. Rev. Mater.* **2022**, *7*, 653.
[20] A. N. Morozovska, E. A. Eliseev, M. D. Glinchuk, R. Blinc, *Phys. Rev. B* **2010**, *81*, 092101.
[21] V. B. Nascimento, B. V. daCosta, J. P. Rino, *Appl. Phys. A* **2020**, *126*, 744.
[22] E. Bousquet, N. A. Spaldin, P. Ghosez, *Phys. Rev. Lett.* **2010**, *104*, 037601.
[23] M. Djermouni, A. Zaoui, S. Kacimi, N. Benayad, A. Boukortt, *Eur. Phys. J. B* **2018**, *91*, 28.
[24] A. Kashir, H.-W. Jeong, W. Jung, Y. H. Jeong, G.-H. Lee, *Mater. Res. Express* **2019**, *6*, 106321.
[25] V. Goian, R. Held, E. Bousquet, Y. Yuan, A. Melville, H. Zhou, V. Gopalan, P. Ghosez, N. A. Spaldin, D. G. Schlom, S. Kamba, *Commun. Mater.* **2020**, *1*, 74.
[26] S. Pandey, S. Hettler, R. Arenal, C. Bouillet, A. R. Moghe, S. Berciaud, J. Robert, J.-F. Dayen, D. Halley, *Phys. Rev. B* **2023**, *108*, 144423.
[27] H. Mishra, J. Panda, M. Ramu, T. Sarkar, J.-F. Dayen, D. Belotcerkovtceva, M. V. Kamalakar, *J. Phys. Mater.* **2021**, *4*, 042007.
[28] J. F. Sierra, J. Fabian, R. K. Kawakami, S. Roche, S. O. Valenzuela, *Nat. Nanotechnol.* **2021**, *16*, 856.
[29] I. G. Serrano, J. Panda, F. Denoel, Ö. Vallin, D. Phuyal, O. Karis, M. V. Kamalakar, *Nano Lett.* **2019**, *19*, 666.
[30] J. Panda, M. Ramu, O. Karis, T. Sarkar, M. V. Kamalakar, *ACS Nano* **2020**, *14*, 12771.
[31] T. Mairoser, J. A. Mundy, A. Melville, D. Hodash, P. Cueva, R. Held, A. Glavic, J. Schubert, D. A. Muller, D. G. Schlom, A. Schmehl, *Nat. Commun.* **2015**, *6*, 7716.
[32] A. G. Swartz, P. M. Odenthal, Y. Hao, R. S. Ruoff, R. K. Kawakami, *ACS Nano* **2012**, *6*, 10063.
[33] J. Klinkhammer, D. F. Förster, S. Schumacher, H. P. Oepen, T. Michely, C. Busse, *Appl. Phys. Lett.* **2013**, *103*, 131601.
[34] J.-F. Dayen, S. J. Ray, O. Karis, I. J. Vera-Marun, M. V. Kamalakar, *Appl. Phys. Rev.* **2020**, *7*, 011303.
[35] D. A. Solis, A. Hallal, X. Waintal, M. Chshiev, *Phys. Rev. B* **2019**, *100*, 104402.
[36] H. X. Yang, A. Hallal, D. Terrade, X. Waintal, S. Roche, M. Chshiev, *Phys. Rev. Lett.* **2013**, *110*, 046603.
[37] D. Yoon, Y.-W. Son, H. Cheong, *Nano Lett.* **2011**, *11*, 3227.
[38] W. M. Haynes, Ed., *CRC Handbook of Chemistry and Physics*, CRC Press, Boca Raton, **2016**.
[39] X. Hao, J. Zhai, L. B. Kong, Z. Xu, *Progress in Materials Science* **2014**, *63*, 1.
[40] M. Ye Zhuravlev, S. Maekawa, E. Y. Tsymbal, *Phys. Rev. B* **2010**, *81*, 104419.
[41] V. Garcia, M. Bibes, L. Bocher, S. Valencia, F. Kronast, A. Crassous, X. Moya, S. Enouz-Vedrenne, A. Gloter, D. Imhoff, C. Deranlot, N. D. Mathur, S. Fusil, K. Bouzehouane, A. Barthélémy, *Science* **2010**, *327*, 1106.
[42] D. Halley, N. Najjari, H. Majjad, L. Joly, P. Ohresser, F. Scheurer, C. Ulhaq-Bouillet, S. Berciaud, B. Doudin, Y. Henry, *Nat. Commun.* **2014**, *5*, 3167.
[43] E. A. Eliseev, A. N. Morozovska, M. D. Glinchuk, B. Y. Zaulychny, V. V. Skorokhod, R. Blinc, *Phys. Rev. B* **2010**, *82*, 085408.
[44] S. Cao, P. Liu, J. Tang, H. Lu, C.-W. Bark, S. Ryu, C. B. Eom, A. Gruverman, P. A. Dowben, *Appl. Phys. Lett.* **2013**, *102*, 172402.
[45] A. Pirkle, J. Chan, A. Venugopal, D. Hinojos, C. W. Magnuson, S. McDonnell, L. Colombo, E. M. Vogel, R. S. Ruoff, R. M. Wallace, *Appl. Phys. Lett.* **2011**, *99*, 122108.
[46] B. T. Matthias, R. M. Bozorth, J. H. Van Vleck, *Phys. Rev. Lett.* **1961**, *7*, 160.
[47] K. Ahn, A. O. Pecharsky, K. A. GschneidnerJr., V. K. Pecharsky, *J. Appl. Phys.* **2005**, *97*, 063901.

[48] H. A. Eick, N. C. Baenziger, L. Eyring, *J. Am. Chem. Soc.* **1956**, *78*, 5147.
[49] S. Q. A. Shah, M. Annaorazov, G. Rimal, J. Wang, M. F. Borunda, J. Tang, A. J. Yost, *ACS Appl. Mater. Interfaces* **2023**, *15*, 10141.
[50] P. Liu, J. Tang, *J. Phys.: Condens. Matter* **2013**, *25*, 125802.
[51] N. J. C. Ingle, I. S. Elfimov, *Phys. Rev. B* **2008**, *77*, 121202.
[52] G. Song, M. Ranjbar, D. R. Daughton, R. A. Kiehl, *Nano Lett.* **2019**, *19*, 7112.
[53] N. Konstantinov, A. Tauzin, U. N. Noumbé, D. Dragoe, B. Kundys, H. Majjad, A. Brosseau, M. Lenertz, A. Singh, S. Berciaud, M.-L. Boillot, B. Doudin, T. Mallah, J.-F. Dayen, *J. Mater. Chem. C* **2021**, *9*, 2712.
[54] J.-F. Dayen, N. Konstantinov, M. Palluel, N. Daro, B. Kundys, M. Soliman, G. Chastanet, B. Doudin, *Mater. Horiz.* **2021**, *8*, 2310.